Articles

Solution Structure of BmBKTx1, a New BK_{Ca}[1] Channel Blocker from the Chinese Scorpion *Buthus martensi* Karsch[†,‡]

Zheng Cai,[§,||] Chenqi Xu,[||,⊥] Yingqi Xu,[§] Wuyuan Lu,[+] Cheng-wu Chi,[⊥,@] Yunyu Shi,[§] and Jihui Wu*[,§]

Laboratory of Structural Biology, School of Life Science, University of Science and Technology of China, Hefei, Anhui, PRC, Shanghai Institute of Biochemistry and Cell Biology, Chinese Academy of Sciences, Yue-Yang Road 320, Shanghai 200031, PRC, Institute of Human Virology, University of Maryland, 725 West Lombard Street, Baltimore, Maryland 21201, and Institute of Protein Research, Tong-Ji University, Shanghai 200092, PRC

Received August 7, 2003; Revised Manuscript Received November 24, 2003

ABSTRACT: BmBKTx1 is a 31-amino acid peptide identified from the venom of the Chinese scorpion *Buthus martensi* Karsch, blocking high-conductance calcium-activated potassium channels. Sequence homology analysis indicates that BmBKTx1 is a new subfamily of short-chain α-KTx toxins of the potassium channel, which we term α-KTx19. Synthetic BmBKTx1 was prepared by using solid-phase peptide synthesis. Two-dimensional NMR spectroscopy techniques were used to determine the solution structure of BmBKTx1. The results show that the BmBKTx1 forms a typical cysteine-stabilized α/*β* scaffold adopted by most short-chain scorpion toxins. The structure of BmBKTx1 consists of a two-stranded antiparallel *β*-sheet (residues 20−29) and an α-helix (residues 5−15). The three-dimensional structure of BmBKTx1 was also compared with those of two function-related scorpion toxins, charybdotoxin (ChTx) and BmTx1, and their structural and functional implications are discussed.

Potassium channels play a major role in a variety of physiological processes such as cell excitability, release of neurotransmitters, secretion of hormones, signal transduction, cell volume regulation, and neuronal integration (*1*). According to their physiology function, potassium channels can be divided into either voltage-gated or ligand-gated channels. Despite the large amount of information about K^+ channels that has been accumulated in the past few years, the important issue of how the different K^+ channels have different physiological function still remains unresolved. To address this question, it is necessary to find selective probes with high affinity that target specific channels. Scorpion venoms contain various polypeptides that particularly affect the permeability of different ion channels in cell membranes (*2*). Up to now, different peptides related to the K^+ channel toxin family have been isolated from the venom of *Buthus martensi* Karsch. Calcium-activated potassium channels are a diverse class of K^+ channels that share a common feature, being gated by intracellular Ca^{2+}. On the basis of differences in single-channel conductance, pharmacological properties, and voltage dependence of channel opening, they can be further divided into three subclasses: small-conductance (10−20 pS, SK_{Ca}),[1] intermediate-conductance (25−100 pS), and high-conductance (100−300 pS, BK_{Ca}) channels (*3*). In the past few years, many short-chain scorpion neurotoxins exhibiting different specificities and potencies for these three subclasses of K^+ channels were discovered. Among them, charybdotoxin, iberiotoxin, kaliotoxin, and noxiustoxin interfere with BK_{Ca} channels (*4*−*7*), while Leiurotoxin I, P05, P01, and BmP02 act on SK_{Ca} channels (*8*−*11*).

To investigate the structure−function relationship, the structures of several short-chain scorpion toxins targeting K^+ channels have been determined by NMR spectroscopy. They include charybdotoxin (*12*), iberiotoxin (*13*), noxiustoxin (*14*), kaliotoxin (*15*), margatoxin (*16*), P05 (*17*), BmP02 (*18*), and tityustoxin K-α (*19*). The structural studies revealed a common global fold for all these neurotoxins stabilized by three disulfide bridges. Despite their sequence variations, these short-chain scorpion toxins all possess an N-terminal α-helix connected to a C-terminal two- or three-stranded antiparallel *β*-sheet via a turn or a loop.

[†] This work is supported by the Chinese National Fundamental Research Project (Grant G1999075605), the Chinese National Natural Science Foundation (Grants 30270293 and 30121001), the National High Technology Research and Development Program of China (Grant 2001AA233021), the Key Project of the National High Technology Research and Development Program of China (Grant 2002BA711A13), and the Pilot Project of the Knowledge Innovation Program of the Chinese Academy of Science (Grant KSCX1-SW-17).

[‡] The atomic coordinates of BmBKTx1 havebeen deposited in the Brookhaven Protein Data Bank as entry 1Q2K.

* To whom correspondence should be addressed. Fax: +86-551-3603754. Telephone: +86-551-3603745. E-mail: wujihui@ustc.edu.cn.

[§] University of Science and Technology of China.

[||] These authors contributed equally to this work.

[⊥] Chinese Academy of Sciences.

[+] University of Maryland.

[@] Tong-Ji University.

[1] Abbreviations: NMR, nuclear magnetic resonance; SK_{Ca} channel, low-conductance calcium-activated potassium channel; BK_{Ca} channel, high-conductance calcium-activated potassium channel.

10.1021/bi035412+ CCC: $27.50
Published on Web 03/10/2004

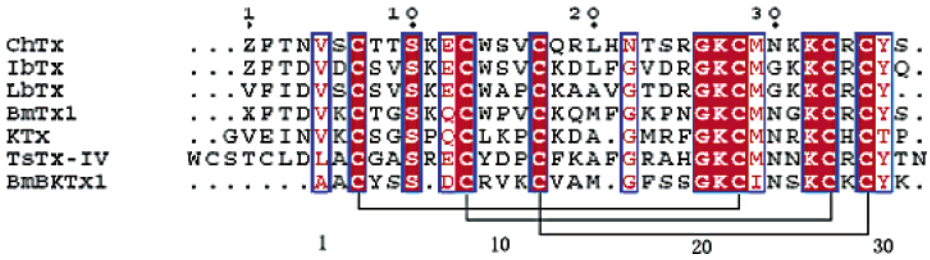

FIGURE 1: Sequence alignment of BmBKTx1 with six other BK_{Ca} channel blockers generated using Clustal-W (*20*) and ESPript (*21*). Three-dimensional solution structures for the first five of them have been determined. Residues that are identical have a red background; those that are highly conserved are depicted with red letters. The sequence numbers at the top are based on the sequence of ChTx, while the sequence numbers at the bottom are based on the sequence of BmBKTx1. The conserved disulfide bridges are shown.

BmBKTx1 was recently isolated and purified, and its sequence was determined (personal communication with C.-w. Chi) from the venom of the Chinese scorpion *B. martensi* Karsch, a species widely distributed in northwestern China, Mongolia, and Korea. The sequence homology analysis indicates that BmBKTx1 is a new subfamily of short-chain α-KTx toxins blocking the potassium channel, which we term α-KTx19. This toxin has been demonstrated to be a selective blocker of BK_{Ca} channels in the locust dorsal unpaired media (DUM) neuron and also could block the cloned BK channel expressed in mammalian cells (personal communication with C.-w. Chi). BmBKTx1 is the shortest BK_{Ca} blocker from the scorpion venom, composed of only 31 residues. Other scorpion BK_{Ca} blockers are all longer than 37 residues. BmBKTx1 is a highly basic toxin with six positively charged residues (five Lys residues and one Arg) and only one negatively charged residue (Asp). The sequence alignment of BmBKTx1 with six other BK_{Ca} channel blockers from scorpion is shown in Figure 1.

As shown in Figure 1, six Cys residues (C3, C8, C12, C22, C27, and C29) and one Ser (S6) are conserved, and the C-terminal regions are also similar among these toxins. Despite this similarity, the sequence of BmBKTx1 exhibits some unique properties. For instance, no positively charged residues precede Cys8 in BmBKTx1, whereas other toxins all contain Lys or Arg in the corresponding region. BmBKTx1 possesses Ile at position 23 instead of Met in all other BK_{Ca} toxins, and a quite diverse sequence in the loop between C12 and C22. These differences make the determination of three-dimensional solution structure of BmBKTx1 meaningful. Here we report the solution structure of BmBKTx1 determined by NMR spectroscopy. Structural studies of scorpion toxins help to elucidate the mechanisms of action of toxins, and are also important for drug design and therapeutic intervention (*22*).

MATERIALS AND METHODS

Chemical Synthesis of BmBKTx1. BmBKTx1 was synthesized on Boc-Lys(2ClZ)-OCH_2-PAM resin using a custom-modified, machine-assisted chemistry tailored from the published in situ DIEA neutralization/HBTU activation protocol for Boc solid-phase peptide synthesis (*23*). The following side-chain protections were used: Cys(4MeBzl), Asp(OcHxl), Lys(2ClZ), Asn(xanthyl), Arg(tosyl), Ser(Bzl), and Tyr(BrZ). After chain assembly, the peptide was cleaved and deprotected by HF for 1 h in the presence of a 5% *p*-cresol/thiocresol mixture (1:1) at 0 °C, followed by precipitation with cold ether. The crude product was purified by reversed-phase HPLC to homogeneity, and its molecular weight was ascertained by electrospray ionization mass spectrometry.

Oxidative folding of purified BmBKTx1 was performed by dissolving the peptide at 3 mg/mL in 6 M Gu-HCl containing 18 mM reduced glutathione and 1.8 mM oxidized glutathione, followed by a rapid 6-fold dilution with 0.25 M $NaHCO_3$. Folding and/or disulfide formation proceeded quantitatively at room temperature overnight, and the final product was purified by HPLC and lyophilized.

Sample Preparation. Synthetic BmBKTx1 was dissolved to a final concentration of 3 mM in 450 μL of a 90:10 (v/v) H_2O/D_2O mixture. The pH was then adjusted to 5.0 (uncorrected for the isotope effect). After a set of NMR experiments, this sample was lyophilized and redissolved in 99.96% D_2O for the rest of the experiments.

NMR Spectroscopy. All NMR measurements were performed at 300 K on a Bruker DMX500 spectrometer, and self-shielded *z*-axis gradients were used. Two-dimensional TOCSY, DQF-COSY, and NOESY spectra were acquired in H_2O and D_2O using the States−TPPI method to achieve F_1 quadrature detection. Typically, 700 free induction decays of 2048 data points were collected per experiment. The spectral width was set to 5000 Hz. TOCSY spectra were recorded with a spin lock time of 73 ms, while mixing times of 100 and 200 ms were used for NOESY to identify spin diffusion effects. To minimize the contribution from zero quantum coherence, the NOESY mixing time was varied randomly by 10% (*24*). Low-power presaturation and WATERGATE (*25*) were used to suppress the water signal in these experiments. The amide proton exchange experiments were carried out immediately after dissolution of this peptide into D_2O on an ice bath. The disappearance of NH signals was followed at 300 K. Ten one-dimensional spectra were acquired continuously over the first 10 min. Then several TOCSY spectra, taken at approximately 0.5, 1, 1.5, 2, 3, 4, 6, 8, 12, 20, and 28 h, were recorded sequentially.

Data Processing. Spectra were processed with Bruker's UXNMR software. The matrices were transformed to a final size of 2048 points in both dimensions. The signal was multiplied by a shifted sine bell window in both dimensions before Fourier transformation. Baseline distortions were corrected using the FLATT procedure.

Spectral Analysis. Spin system identification and sequential assignment were done using the Wüthrich strategy (*26*), aided by the XEASY software (*27*).

Experimental Restraints. NOE intensities were obtained mainly from a NOESY spectrum with a mixing time of 100 ms on the fully protonated sample. For those peaks between two aliphatic protons, with which zero-quantum effects and/or the overlap problem in this spectrum interfered severely, integration was carried out on a NOESY spectrum recorded in D_2O with a mixing time of 200 ms. Buildup curves of the NOE intensity were checked, and no severe spin diffusion effect was found up to 200 ms (data not shown). The scaling factors for different spectra were chosen carefully after comparing the integration for a set of well-separated strong peaks. All the NOEs were calibrated to distance upper limits according to the well-known r^{-6} relation and known distances; i.e., $d_{\alpha N}$ (in a β-strand) = 2.2 Å, and d_{NN} = 3.3 Å between two strands of antiparallel β-sheet. To allow for possible fluctuations, the distance restraints derived from side-chain cross-peaks and weak backbone cross-peaks were lengthened to 4.0 or 5.0 Å. An additional 0.5 Å was added to those distances corresponding to methyl protons. No lower limit was imposed explicitly.

The $^3J_{HN\alpha}$ values were obtained by measuring the division of cross-peaks on TOCSY parallel to F_2 or by using the INFIT routine (*28*) provided by XEASY. Then they were converted to ϕ angle constraints as $-65° \pm 25°$ (<6.5 Hz), $-120° \pm 25°$ (>9 Hz), and $-120° \pm 35°$ (>8 Hz).

Structure Calculations. Simulated annealing of the BmBKTx1 structures based on geometric restraints (bond length, bond angle, and improper dihedral angle), simple repulsion nonbonded interactions, and all the restraints (NOE, dihedral angle, and hydrogen bond) derived from NMR spectra were used in CNS (*29*). The simulation started from an extended conformation of BmBKTx1 with its disulfide bridges removed. The simulation was carried out in torsion angle space at first, which involved 1000 steps (the time step being 0.015 ps) at 50 000 K and 1000 more steps of cooling the system slowly to 0 K (the time step being 0.015 ps and the temperature step being 250 K). A second slow-cool annealing was then carried out in Cartesian space with the system temperature decreasing from 2000 to 0 K in 3000 steps (the time step being 0.005 ps and the temperature step being 25 K). Finally, a 3000-step Powell minimization was performed to obtain the last conformation. This conformation was checked for violations of geometric and experimental restraints and atom overlapping. If there were no severe restraint violation and/or atom overlapping, it was accepted by the program as a possible solution. Regardless of whether this conformation was accepted, it would be used as the starting conformation for the next cycle of simulation. The initial velocities were randomly set according to the Maxwell distribution at the starting temperature; therefore, the sampling would not be trapped in a local minimum. The simulation was repeated until enough conformations had been accepted. During one particular cycle, the weighting factor for the van der Waals energy was increased from 0.1 to 4.0, which also aided in transferring the system to different conformations at the beginning of the simulation.

Although this procedure is not an iterative one itself, we repeated it for several trials. There were some NOE peaks that could not be assigned unambiguously at the beginning of our calculation due to chemical shift overlapping. Some of them were imposed as summation-averaged distance restraints (*30*), while the others were not used until they could be assigned with the help of intermediate structures.

RESULTS AND DISCUSSION

Sequential Assignment. Spin systems were identified on the basis of both the TOCSY and DQF-COSY spectra. At 300 K, all 30 spin systems were found without significant overlapping, except for the first alanine. The unique Arg9, Met15, and Ile23 residues were identified according to the patterns of their cross-peaks on TOCSY and DQF-COSY spectra. We also identified two glycine (Gly16 and Gly20), five lysine, two alanine, and two valine residues based on their special patterns of cross-peaks. The three aromatic residues (Tyr4, Phe17, and Tyr30) were identified using the intraresidual NOE cross-peaks between its two Hβ protons and the Hδ protons on the benzene ring. There were 16 AMX spin systems left, which could be identified only in the sequential assignment via the NOESY spectra. Starting from Arg9, we linked it down to Ala2, starting from Met15 to Val10 and starting from Ile23 up to Asn24 and down to Gly16. Besides the assigned Tyr4 and Phe17, there was only one aromatic residue (Tyr30) left. From Tyr30, we linked the sequence up to Lys31 and down to Ser25. All the above linkage was based on the Hα−HN$_{i,i+1}$ connectivities, and later confirmed by HN−HN$_{i,i+1}$ connectivities or Hβ−HN$_{i,i+1}$ connectivities (Figure 2). The assignment of one spin system, which comprised only one cross-peak due to the Hα−Hβ overlap, to a Ser residue was verified by the final complete assignment of all the protons. Finally, a complete assignment of all the protons was obtained (see Table S1 of the Supporting Information).

Coupling Constants. Twenty-seven $^3J_{HN\alpha}$ values were obtained as listed in Table S2 of the Supporting Information. Twenty-one of them were converted into ϕ angle constraints. Among the four residues for which we failed to obtain coupling constants, there were Ala1, Gly16, Gly20, and Ser5, for which no suitable peaks with a sufficient signal-to-noise ratio could be used.

Secondary Structures. Analysis of the sequential and medium-range NOE intensities together with the chemical shifts and coupling constant values helped us to depict the secondary structure of BmBKTx1 (Figure 2). In the N-terminus, a stretch of Hα−HN$_{i,i+3}$ and three Hα−HN$_{i,i+4}$ connectivities in BmBKTx1 was found, and a stretch of strong HN−HN$_{i,i+1}$ NOEs in this region was also observed, which indicated that there was an α-helix between residues 5 and 15. This was confirmed by the relatively small coupling constants for the residues in this region. Two stretches of strong sequential Hα−HN NOEs indicated two extended regions running from residue 19 to 23 and from residue 25 to 30. HN−HN connectivities were identified between residues 19 and 30, 21 and 30, 22 and 28, and 23 and 26. Thus, we suggested that an antiparallel β-sheet centered at residues 24 and 25 ran from residue 20 to 29. This was also confirmed by the relatively large coupling constants for the residues located in the two strands.

Hydrogen Bonds. The rates of exchange of amide protons with solvents were measured. Amide protons present after exchange for 16 h were considered slowly exchanging amide protons, which may be engaged in hydrogen bonds. In our experiments, the HN of residues 10−13, 15, 21, and 28 gave

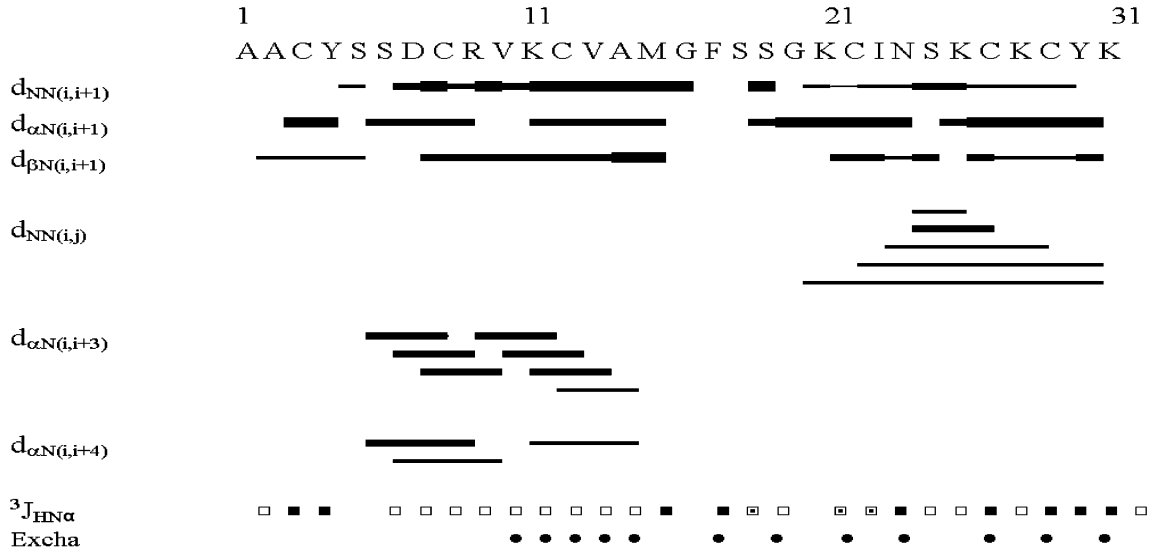

FIGURE 2: Sequence of BmBKTx1 and NMR data used for secondary structure identification. The data were derived from NOESY and DQF-COSY spectra recorded at pH 5.0 and 300 K. The H−D exchange experiments were also performed at 300 K. $^3J_{HN\alpha} \leq 6.5$ Hz (□); 6.5 Hz $\leq {}^3J_{HN\alpha} \leq 8$ Hz (⊡), and $^3J_{HN\alpha} > 8$ Hz (■).

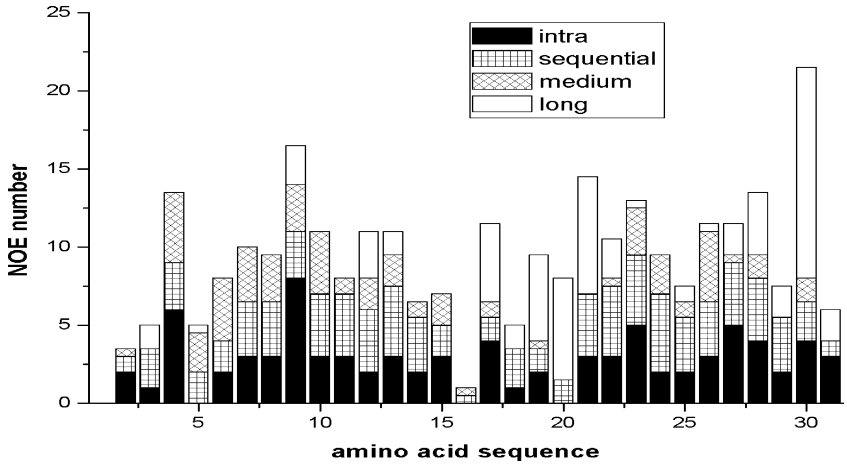

FIGURE 3: Plot of the number of NOE constraints per residue used in the calculation of the BmBKTx1 structure vs the sequence of BmBKTx1. Filled, striped, cross-hatched, and empty bars represent intraresidual, sequential, medium-range, and long-range NOEs, respectively.

rise to cross-peaks on the TOCSY spectrum after exchange for 16 h. Some preliminary calculations confirmed the existence of the α-helix between residues 5 and 15, and indicated that the HN groups of residues 10−13 and 15 formed hydrogen bonds with the CO group of residues 6−9 and 11, respectively. Thus, we included these five hydrogen bonds in the structure calculation at an early stage. The existence of a β-sheet from residue 20 to 29 was also confirmed during the calculation, and we found that hydrogen bonds were formed between residues 21 and 28. These two hydrogen bonds were also added as restraints. Other amide protons, which showed relatively quick rates of H−D exchange, were not included in the structure calculation.

Stereospecific Assignment. We have tried to make stereospecific assignments for β-methylene protons according to intraresidue and sequential NOEs using the HABAS (*31*) routine in DYANA (*32*). Only the stereospecific assignment of HB protons of Cys8 was obtained. So, for all the other prochiral pairs of protons and the other ambiguous NOEs, their r^{-6} summation-averaged distances were constrained during the simulation, with the upper limit converted from the sum of the two NOE intensities.

Structure Calculations. The final set of constraints contained 84 intraresidue, 90 sequential, 50 medium-range, and 63 long-range distance constraints (Figure 3), together with 21 angle constraints and 14 distance constraints derived from seven hydrogen bonds and three disulfide bonds. From the 100 accepted conformations, the 20 structures with minimal NOE violations and the lowest total energy were selected. These 20 conformations, together with their minimized average conformation, formed our solution for the structure of BmBKTx1. These 20 conformations were in good agreement with the experimental data with no distance violations larger than 0.3 Å and no angle violations of more than 5°. Only four of these conformations had one distance violation larger than 0.20 Å. Figure 4 showed the backbone and heavy atom rmsd values for the 20 selected structures with respect to the mean structure. The covalent geometry was elucidated as indicated by the low-energy values of the bond lengths and valence angles. The negative van der Waals

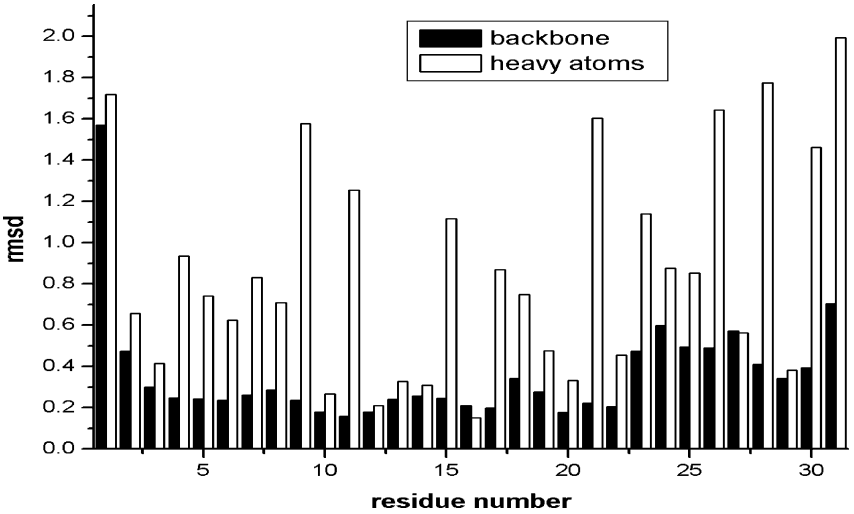

FIGURE 4: Backbone and heavy atom rmsd values for the 20 selected structures with respect to the mean structure.

Table 1: Structural Statistics for BmBKTx1

rmsd from experimental restraints	
NOE distance restraints (Å)	0.032 ± 0.002
cdih restraints (Å)	0.31 ± 0.05
rmsd from idealized geometry	
bonds (Å)	0.0036 ± 0.00017
angles (deg)	0.516 ± 0.017
rmsd from mean coordinates	
backbone atoms (Å)	0.47 ± 0.21
heavy atoms (Å)	1.19 ± 0.33

energy indicated the absence of nonbonded contacts. The van der Waals energy could be lowered dramatically after 100 steps of Powell minimization considering the complete van der Waals energy and electrostatic energy, while other energies were increased slightly (data not shown). A Ramachandran plot was produced by PROCHECK-NMR (*33*), which showed that 82.8% of the residues are in the most favored regions and 11.1% and 6.1% in additional and generously allowed regions, respectively (Figure S1 of the Supporting Information).

Table 1 lists the structure statistics for BmBKTx1. The rms deviations calculated over the backbone heavy atoms and all heavy atoms of the whole molecule were 0.47 ± 0.21 and 1.19 ± 0.33 Å, respectively.

Structure Description. Figure 5b shows the ribbon representation for the minimized average structure of BmBKTx1. Like other short-chain scorpion toxins, BmBKTx1 possesses an α-helix (residues 5−15) and an antiparallel β-sheet (residues 20−29) interlocked by two disulfide bridges.

The α-helix, running from residue 5 to 15, was well-defined, as evidenced by the low rmsd for this region. We observed the relatively slow H−D exchange rates of the HNs from residues 10−15, suggesting that strong H-bonds form between the HN_{i+4} group and the CO_i group in this region to stabilize the helix structure.

The β-hairpin was also well-defined, as evidenced by the low rmsd for this region. The sheet was right-hand-twisted. The turn, as analyzed by the criteria described by Chou *et al.* (*34*), is classified as a type IV β-turn.

Classification. The family of K^+ channel specific toxins comprises three structurally distinct groups, designated as α-KTx, β-KTx, and γ-KTx. Peptides belonging to the α-KTx group are the best-studied toxins. On the basis of the primary structure homology, Tytgat *et al.* (*36*) classified the short-chain scorpion K^+ toxins into 12 subfamilies named α-KTx1−α-KTx12 in 1999. In 2002, Goudet *et al.* (*37*) updated this classification to 17 subfamilies. Batista *et al.* (*38*) defined the 18th subfamily in 2002. As seen in Figure 6, the amino acid sequence of BmBKTx1 was only slightly homologous with those of the 18 other known subfamilies. According to their disulfide pattern and genomic organization, it can be inferred that BmBKTx1 belongs to a new subfamily of α-KTx toxins. Thus, we classified BmBKTx1 as the first member of the 19th subfamily. This new scorpion toxin subfamily will provide more information for further research with these toxins.

Comparison with ChTx and BmTx1. ChTx and BmTx1 are two other well-known scorpion toxins that block BK_{Ca} K^+ channels. Both of them are members of the first α-KTx subfamily. Possani (*39*) recently indicated that amino acid residues situated at the β-hairpin of α-KTx subfamilies 1−3 may be involved in the interaction with the K^+ channel. Eight residues of ChTx (S10, W14, R25, K27, M29, N30, R34, and Y36) were found to be crucial for binding to the K^+ channel. Four of them (S10, K27, N30, and Y36) are conserved in BmBKTx1, while M29 and R34 are conservatively replaced in BmBKTx1 with I23 and K28, respectively. Five of them (K27, M29, N30, R34, and Y36) are located in the β-hairpin region, which indicates that they may be important for the interaction of BmBKTx1 with the BK_{Ca} channels, although we had no experimental evidence until now. Figure 5d shows the backbone superposition of BmBKTx1 with the corresponding C-termini of ChTx and BmTx1. Figure 7 shows the comparison of the ribbon structures and the electrostatic surfaces of BmBKTx1, ChTx, and BmTx1. As shown in the figures, despite the small β-strand in the N-terminus of ChTx and BmTx1, the α-helix and β-sheet of BmBKTx1 resemble the corresponding parts of ChTx (with a backbone rmsd of 2.64 Å) and BmTx1 (with a backbone rmsd of 2.91 Å), suggesting that the short N-terminal segment of ChTx and BmTx1 might be related to the functional difference, such as the channel selectivity, between BmBKTx1 and the other two. As seen from the electrostatic surface, there is a negatively charged residue

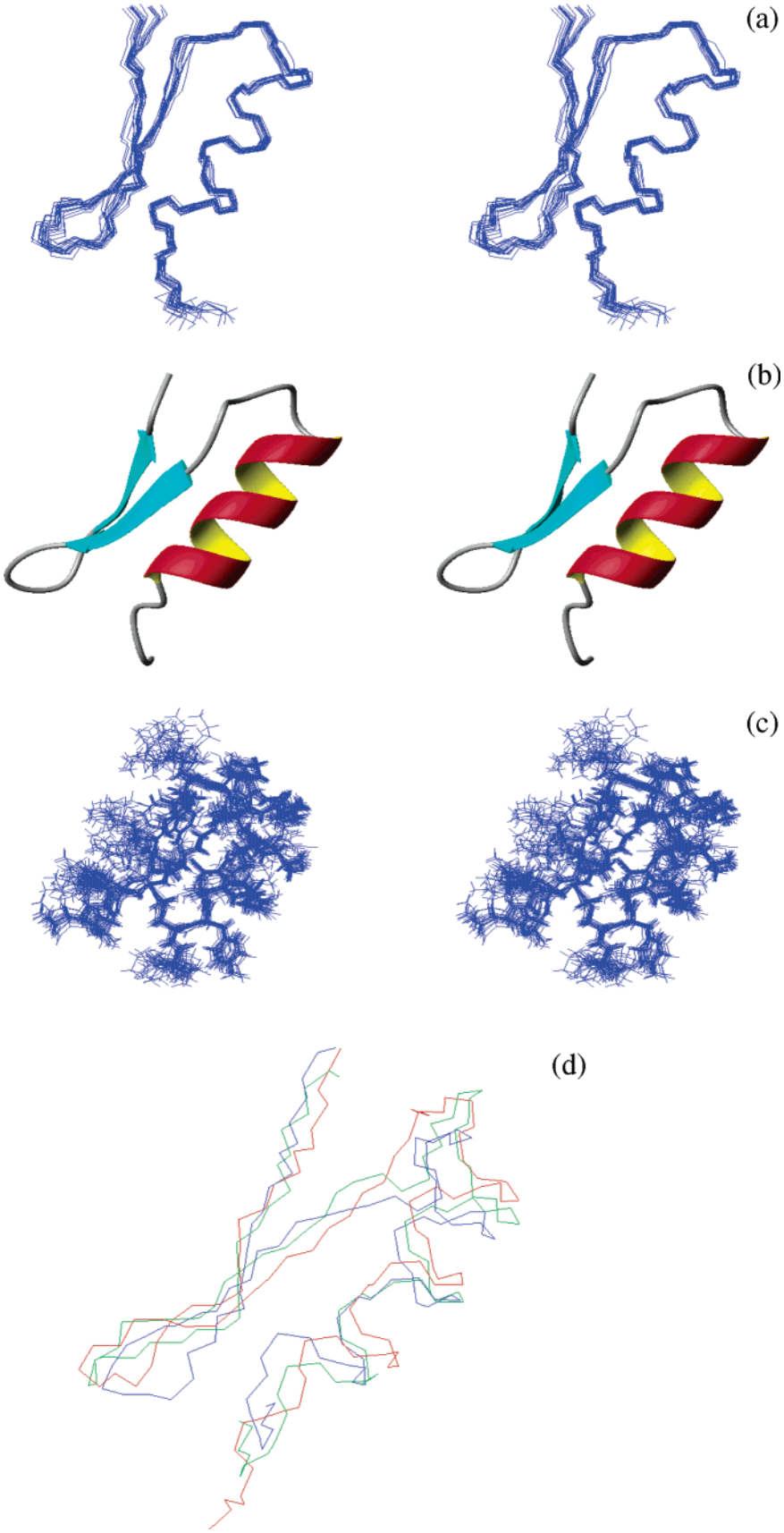

FIGURE 5: Stereoview of (a) the backbone superimposition of the 20 models for BmBKTx1, (b) the ribbon representation of the minimized average structure of BmBKTx1, (c) the all atom superimposition of the 20 models for BmBKTx1, and (d) the backbone superposition of BmBKTx1 (red) with the 31 corresponding C-terminal residues of ChTx (green) and BmTx1 (blue) (structure derived from PDB entries 2CRD and 1BIG, respectively). This figure was produced with MOLMOL (*35*).

in the helical region in both ChTx and BmBKTx, but not in BmTx1, which suggests that this negative charge might also be functionally dispensable. On the other hand, the C-terminal part of all these three toxins, especially in the

```
α-KTx1.1  ChTx        ---ZFTNVSCTTSKECWSVCQRLHN-TSRGKCMN-KKCRCYS-    35%
α-KTx2.1  NTx         ---TIINVKCTSPKQCSKPCKELTGSSAGAKCMN-GKCKCYNN    28%
α-KTx3.1  KTx         --GVEINVKCSGSPQCLKPCKDA-G-MRFGKCMN-RKCHCTPK    32%
α-KTx4.1  TyKalpha    ---VFINAKCRGSPECLPKCKEAIG-KAAGKCMN-GKCKCYP-    43%
α-KTx5.1  LeTxI       -------AFCN-LRMCQLSCRSL-G-LL-GKCIG-DKCECVKH    41%
α-KTx6.1  Pi1         ------LVKCRGTSDCGRPCQQQTG-CPNSKCIN-RMCKCYGC    40%
α-KTx7.1  Pi2         ------TISCTNPKQCYPHCKKETG-YPNAKCMN-RKCKCFGR    31%
α-KTx8.1  P01         -------VSCE---DCPEHCSTQKA---QAKCDN-DKCVCEPI    31%
α-KTx9.1  BmP02       -------VGCE---ECPMHCKGKNA---KPTCDD-GVCNCN-V    19%
α-KTx10.1 CoTx1       -------AVCV-YRTCDKDCKRR-G-YRSGKCIN-NACKCYPY    47%
α-KTx11.1 PBTx1       --DEEPKESCS-DEMCVIYCKGE-E-YSTGVCDGPQKCKCSD-    27%
α-KTx12.1 TsTxIV      WCSTCLDLACGASRECYDPCFKAFG-RAHGKCMN-NKCRCYTN    34%
α-KTx13.1 Tc1         --------AC---GSCRKKCK------GSGKCIN-GRCKCY--    52%
α-KTx14.1 BmSKTx1     ---TPFAIKCATNADCSRKCPGN-----PP-CRN-GFCACT--    25%
α-KTx15.1 BmTx3A      --ZVETNVKCQG-GSCASVCRKAIG-VAAGKCIN-GRCVCYP-    32%
α-KTx16.1 Tamapin     -------AFCN-LRRCELSCRSL-G-LL-GKCIG-EECKCVPY    38%
α-KTx17.1 BmKK4       ------QTQCQSVRDCQQYCLTP------DRCSY-GTCYCKTT    21%
α-KTx18.1 Tc32        ---TGPQTTCQ-AAMCEAGCKGL--GKSMESCQG-DTCKCKA-    26%
α-KTx19.1 BmBKTx1     -------AACY-SSDCRVKCVAM-G-FSSGKCIN-SKCKCYK-    100%
```

FIGURE 6: Comparative alignment of selected short-chain scorpion neurotoxins representing the different subfamilies. Sequences were obtained from the SWISS-PROT database and aligned with Clustal-W (*20*). This figure was produced with BioEdit.

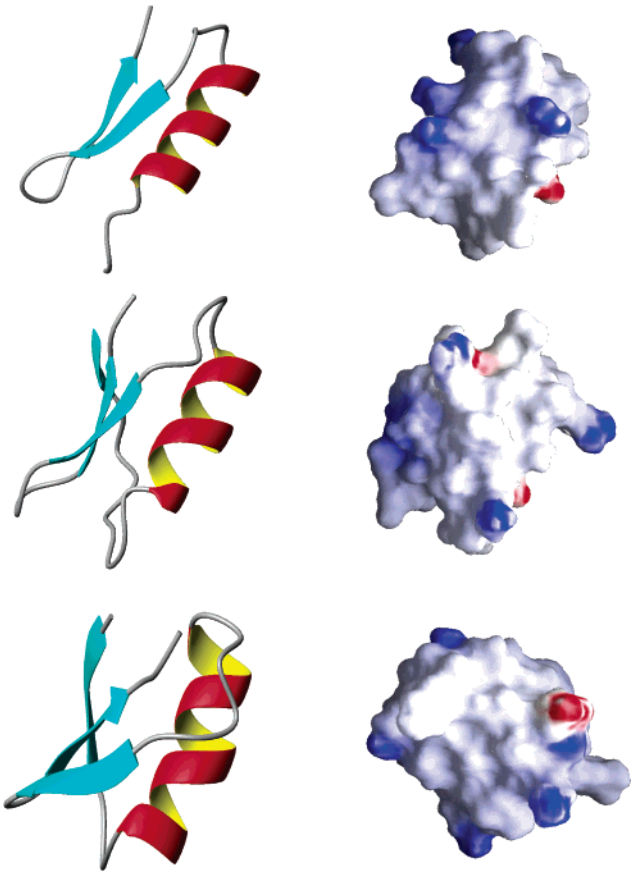

FIGURE 7: Comparison of the ribbon structure and the electrostatic surface of BmBKTx1 and two structurally and functionally related scorpion toxins, ChTx and BmTx1 (BmBKTx1, ChTx, and BmTx1 from top to bottom). ChTx and BmTx1 coordinates were obtained Protein Data Bank entries 2CRD and 1BIG, respectively. The electrostatic surface panels were produced with GRASP (*40*).

β-sheet, is highly positively charged, which is believed to be related to the binding of the toxin with the voltage-gated K^+ channel.

In conclusion, the sequence homology analysis indicates that BmBKTx1 constitutes a new subfamily of short-chain α-KTx toxins, which we term α-KTx19. The determination of the three-dimensional structure of BmBKTx1 and its comparison with other related blockers of the BK_{Ca} channels suggest that the short N-terminal segment might be related to the functional difference between them.

ACKNOWLEDGMENT

We thank Dr. P. Güntert and Prof. K. Wüthrich for providing DYANA, Dr. C. Bartels and Prof. K. Wüthrich for providing XEASY, Dr. R. Koradi and Prof. K. Wüthrich for providing MOLMOL, and Dr. A. T. Brünger for providing CNS.

SUPPORTING INFORMATION AVAILABLE

Chemical shifts of BmBKTx1 protons (Table S1), 27 $^3J_{HN\alpha}$ values that were obtained and the 21 that were selected as ϕ angle constraints (Table S2), Procheck analysis results of the calculated structure of BmBKTx1 (Figure S1), and the sequential connectivity in the Hα−HN and HN−HN regions of the helix and sheets (Figures S2 and S3). This material is available free of charge via the Internet at http://pubs.acs.org.

REFERENCES

1. Coetzee, W. A., *et al.* (1999) *Ann. N.Y. Acad. Sci. 868*, 233−285.
2. Catterall, W. A. (1980) *Annu. Rev. Pharmacol. Toxicol. 20*, 15−43.
3. Gregory, J. K., Hans-Gunther, K., Reid, J. L., Owen, B. M., and Maria, L. G. (1996) *J. Bioenerg. Biomembr. 28* (3), 255−267.
4. Gimenez, G., Navia, M. A., Reuben, J. P., Katz, G. M., Kaczorowshi, G. J., and Garcia, M. L. (1988) *Proc. Natl. Acad. Sci. U.S.A. 85*, 3329−3333.
5. Galvez, A., Gimenez, G., Reuben, J. P., Ray-Contanain, L., Feigenbaum, P., Kaczorowski, G. J., and Garcia, M. L. (1990) *J. Biol. Chem. 265*, 11083−11090.
6. Crest, M., Jacquet, G., Gola, M., Zerrouk, H., Benslimane, A., Rochat, H., Mansuelle, P., and Martin-Eauclaire, M. F. (1992) *J. Biol. Chem. 267*, 1640−1647.
7. Possani, L. D., Martin, B. M., and Svendsen, I. (1982) *Carlsberg Res. Commun. 47*, 285−289.

8. Auguste, P., Hugues, M., Grave, B., Gesquiere, J.-C., Maes, P., Tartar, A., Romey, G., Schweitz, H., and Lazdunski, M. (1990) *J. Biol. Chem. 265*, 4753−4759.
9. Zerrouk, H., Mansuelle, P., Benslimane, A., Rochat, H., and Martin-Eauclaire, M. F. (1993) *FEBS Lett. 320*, 189−192.
10. Zerrouk, H., Laraba-Djebari, F., Fremont, V., Meki, A., Darbon, H., Mansuelle, P., Oughideni, R., Van Rietschoten, J., Rochat, H., and Martin-Eauclaire, M. F. (1996) *Int. J. Pept. Protein Res. 48*, 514−521.
11. Zhu, S., Li, W., Zeng, X., Jiang, D., Mao, X., and Liu, H. (1999) *FEBS Lett. 457* (3), 509−514.
12. Bontems, F., Gilquin, B., Roumestand, C., Menez, A., and Toma, F. (1992) *Biochemistry 31*, 7756−7764.
13. Johnson, B. A., and Sugg, E. E. (1992) *Biochemistry 31*, 8151−8159.
14. Dauplais, M., Gilquin, B., Possani, L. D., Gurrola-Briones, G., Roumestand, C., and Menez, A. (1995) *Biochemistry 34*. 16563−16573.
15. Fernandez, I., Romi, R., Szendeffy, S., Martin-Eauclaire, M. F., Rochat, H., Van Rietschoten, J., Pons, M., and Giralt, E. (1994) *Biochemistry 33*, 14256−14263.
16. Johnson, B. A., Stevens, S. P., and Williamson, J. M. (1994) *Biochemistry 33*, 15061−15070.
17. Meunier, S., Bernassau, J. M., Sabatier, J. M., Martin-Eauclaire, M. F., Rietschoten, J., Cambillau, C., and Darbon, H. (1993) *Biochemistry 32*, 11969−11976.
18. Xu, Y., Wu, J., Pei, J., Shi, Y., Ji, Y., and Tong, Q. (2000) *Biochemistry 39*, 13669−13675.
19. Ellis, K. C., Tenenholz, T. C., Gilly, W. F., Blaustein, M. P., and Weber, D. J. (2001) *Biochemistry 40*, 5942−5953.
20. Thompson, J. D., Higgins, D. G., and Gibson, T. J. (1994) *Nucleic Acids Res. 22*, 4673−4680.
21. Gouet, P., Courcelle, E., Stuart, D. I., and Metoz, F. (1999) *Bioinformatics 15*, 305−308.
22. Menez, A. (1998) *Toxicon 36*, 1557−1572.
23. Schnolzer, M., Alewood, P., Jones, A., Alewood, D., and Kent, S. B. (1992) *Int. J. Pept. Protein Res. 40*, 180−193.
24. Macura, S., Huang, Y., Suter, D., and Ernst, R. R. (1981) *J. Magn. Reson. 43*, 259−281.
25. Piotto, M., Saudek, V., and Sklenar, V. (1992) *J. Biomol. NMR 2*, 661−665.
26. Wüthrich, K. (1986) in *NMR of proteins and nucleic acids*, John Wiley & Sons, New York.
27. Bartels, C., Xia, T.-H., Billeter, M., Güntert, P., and Wüthrich, K. (1995) *J. Biomol. NMR 5*, 1−10.
28. Szyperski, T., Güntert, P., Otting, G., and Wüthrich, K. (1992) *J. Magn. Reson. 99*, 552−560.
29. Brünger, A. T., Adams, P. D., Clore, G. M., Delano, W. L., Gros, P., Grosse-Kunstleve, R. W., Jiang, J.-S., Kuszewski, J., Nilges, M., Pannu, N. S., Read, R. J., Rice, L. M., Simonson, T., and Warren, G. L. (1998) *Acta Crystallogr. D54*, 905−921.
30. Nilges, M. (1993) *Proteins 17*, 297−309.
31. Güntert, P., Braun, W., and Wüthrich, K. (1991) *J. Mol. Biol. 217*, 517−530.
32. Güntert, P., Mumenthaler, C., and Wüthrich, K. (1997) *J. Mol. Biol. 273*, 283−298.
33. Laskowski, R. A., Rullmann, J. A. C., MacArthur, M. W., Kaptein, R., and Thornton, J. M. (1996) *J. Biomol. NMR 8*, 477−486.
34. Chou, P. Y., and Fasman, G. D. (1977) *J. Mol. Biol. 115*, 135−175.
35. Koradi, R., Billeter, M., and Wüthrich, K. (1996) *J. Mol. Graphics 14*, 51−55.
36. Tytgat, J., Chandy, K. G., Garcia, M. L., Gutman, G. A., Martin-Eauclaire, M. F., van der Walt, J. J., and Possani, L. D. (1999) *Trends Pharmacol. Sci. 20*, 444−447.
37. Goudet, C., Chi, C.-W., and Tytgat, J. (2002) *Toxicon 40*, 1239−1258.
38. Batista, C. V. F., Gomez-Lagunas, F., Rodriguez de la Vega, R. C., Hajduc, P., Panyi, G., Gaspar, R., and Possani, L. D. (2002) *Biochim. Biophys. Acta 1601*, 123−131.
39. Rodriguez de la Vega, R. C., Merino, E., Becerril, B., and Possani, L. D. (2003) *Trends Pharmacol. Sci. 24*, 222−227.
40. Nicholls, A., Sharp, K. A., and Honig, B. (1991) *Proteins 11*, 281−296.

BI035412+